EFDA–JET–PR(13)09

T. Craciunescu, A. Murari, B. Sieglin, G. Mathews
and JET EFDA contributors

An Original Spot Detection Method for Large Surveys of Videos in JET

An Original Spot Detection Method for Large Surveys of Videos in JET

T. Craciunescu[1], A. Murari[2], B. Sieglin[3], G. Mathews[4]
and JET EFDA contributors*

JET-EFDA, Culham Science Centre, OX14 3DB, Abingdon, UK

[1]EURATOM-MEdC Association, NILPRP, Bucharest, Romania
[2]Consorzio RFX, Associazione EURATOM-ENEA per la Fusione, Padova, Italy
[3]Max-Planck-Institut für Plasmaphysik, EURATOM-IPP, Garching, Germany
[4]EURATOM-CCFE Fusion Association, Culham Science Centre, OX14 3DB, Abingdon, OXON, UK
** See annex of F. Romanelli et al, "Overview of JET Results",*
(24th IAEA Fusion Energy Conference, San Diego, USA (2012)).

Preprint of Paper to be submitted for publication in
Journal of Nuclear Materials

ABSTRACT

An original spot detection method for large surveys of videos in JET is presented. The method can be used for the automatic identification of spots in JET IR videos and for the assessment of the long term trends in their evolution. This method has been applied to the analysis of a large database of JET IR images collected during the last campaigns of operation with the ILW. The evolution of the spots and their properties, such as size and distribution, can be correlated with macroscopic events, in particular series of intentional disruptions. On the other hand, care must be taken in the interpretation of the results since there is some evidence of toroidal asymmetries in the spot distribution.

1. VIDEOS FOR PLASMA WALL INTERACTIONS ON JET

The widespread use of 2-D sensors for video recording is a characteristic of modern societies. From CCTV cameras to cellular phones, an enormous amount of videos is acquired every day and this trend seems to keep continuing at a high pace. Scientific applications and large experiments show the same increase in the deployment of cameras for various purposes, from scientific investigations to surveying and control. Nuclear Fusion is also showing a similar increased reliance of cameras for diagnostic purposes. As an example nowadays more than 25 cameras are routinely used for imaging on JET in the IR and visible wavelength regions. The applications range from protection of the new JET ITER-like Wall (ILW) to detailed investigations of the plasma wall interactions and of various instabilities. Some of these cameras can produce a quite large amount of data, even of the order of several Gbytes of data per shot. Indeed cameras are nowadays the biggest producers of data on JET.

Videos contain a lot of information but they are notoriously difficult to analyse and interpret. In fusion scientific applications not many automatic tools are available. Therefore in typical studies, a relatively limited number of frames is analysed manually by experts. This fact renders statistical studies of large numbers of videos difficult if not prohibitive in terms of man power. Long term trends are therefore rarely investigated using cameras data.

The present study is devoted to the automatic detection of spots appearing in the images provided by an infra-red (IR) camera system viewing the JET divertor target (KL-9B) from the top of the machine. The main objective consists of determining whether there are long term trends in the number and distribution of these spots some of which are assumed to be dust partcles which have fallen onto the divertor surfaces rather than manufacturing related surface anomalies. The KL-9B camera is located on top of JET vacuum vessel (see figure 1) and is used for the study of temperatures and heat loads on the horizontal tiles of the JET divertor, which are tungsten coated Carbon Fibre Composite (CFC) and bulk tungsten [1]. The camera was manufactured by FLIR ATS (http://www.flir.com) and can operate between 3.5-5μm and up to sampling frequencies of ~20kHz. The full description of this camera is given in Ref. [2].

Typical images recorded by the KL-9B camera are presented in Fig.2. The interpretation of KL-

9B videos presents various difficulties. The frames are characterized by very different brightness, the average pixel gray-level (APGL) lying in the range 40÷140 (for images with 256 gray-levels). For certain levels of brightness, a different distribution of spots can become visible. These spots, characterized by different intensities, may lie on a variable background (see Fig. 3). Moreover, as revealed in Fig. 4, the spots have irregular shapes.

Spot identification and characterization represents the first objective of the developed automatic technique, followed by the retrieval of the evolution of size and distribution during the history of experiments in JET and correlations of these distributions with the physical parameters of the experiments.

With regard to the structure of the paper, next section describes the main spot detection methods reported in the literature and illustrates why they are no adequate to analysis of JET videos. Section 3 reports in detail the characteristics of the original method developed for the automatic analysis of JET IR images. The analysed database and the main results of the survey are the subject of section 4. The main interpretation of the results and the liens of future investigations are discussed in the last section of the paper.

2. OVERVIEW OF IMAGE PROCESSING METHODS FOR SPOT DETECTION

Spot detection tools are used in a wide range of image processing applications. A significant number of methods are already reported for biological and medical applications. One of the most effervescent field is the analysis of proteomics images, used for the study of the complete set of proteins in a cell or organism throughout the entire life-cycle (see e.g. Ref. 2 for a short but comprehensive review). Spot detection of cDNA microarrays is used to identify and quantify different gene-expressions for large-scale analysis (thousands of genes simultaneously) [4-5]. Useful information from the spot parameterisation is obtained also from biological images acquired from fluorescence microscopy-based imaging techniques [6-7] and from images produced by biological immune-microscopy experiments [8]. The non-medical application of the spot detection methods cover a wide range of domains, as it is revealed by the following enumeration which is, of course, far to be comprehensive: SAR imagery [9], technology for printing patterns on silicon (operating in the sub-wavelength regime) [10], analog circuit design [11], load prediction for cloud computing platforms [12].

These extensive and varied efforts generated a broad range of methods for spot identification which may be however grouped in two basic approaches: image segmentation and model-based quantification. The segmentation approach partitions the image into non-overlapping distinct regions and each pixel is labelled as belonging to a certain spot or to the background. The advantage of this approach is that the image is clearly separated into spots and non-spot areas and does not use, in principle, any prior assumption related to the spot nature. The model-based approaches try to model a spot's intensity using a certain analytical function (frequently a Gaussian normal distribution). The spot characteristics are then derived from the model. The main disadvantage consists of the poor representation of irregular spot shapes by simple models.

Among the segmentation approaches the stepwise thresholding and the watershed methods are the most popular.

The stepwise thresholding process [13] consists of using an increasing threshold allowing the splitting of the image in multiple connected areas. This drawback of this method is the high sensitivity to noise, artefacts and non-uniform background.

The watershed transformation (WT) was initially proposed by Beuchner and Lantjeoul [14] and it is used in a wide palette of applications: tracking segmented objects in video, image retrieval from databases, image pattern recognition. It was developed starting from morphological algorithms assuming that the image can be represented as a topographical surface S, where the image grey-levels are associated with altitudes of S. The image, perceived as a relief, is dumped in water and the watershed of the surface S, (WT) is defined as the set of points where two separate ''lakes'' join during the dumping. This transform can be interpreted as an edge detector. Usually it is applied to the gradient image $G(I) \mid \nabla I(S)\mid$ or to the morphological gradient image $G(I) = I \oplus SE - I \ominus SE$ where $\ominus$ is the dilation operator , is the erosion operator and SE is the structuring element. A mean-filter may be applied prior to WT in order to allow a monotonic increasing and thereafter decreasing shape of the spots but this is appropriate only for certain spot shapes. To exclude small regions corresponding to background noise, a threshold may be imposed to the size of the catchment basins. The watershed segmentation provides good results for images characterized by a high signal-to-noise ratio and homogeneity. It provides partitioning of the image even in low contrast conditions. The main drawback of this approach consists of over-segmentation which is an intrinsic problem of the watershed transformation. The main reasons for this effect are the noise and open contours in the gradient image. A series of morphological operations, with the intent of creating approximate foreground and background markers, can be used in principle for removing the spurious parts of the gradient. Meyer and Beucher [15] proposed the so called marker-based watershed, where the number of segmented regions is pre-defined by the number of a set of markers which are placed on the image. However the main drawback is that the automatic placement of the markers is difficult and therefore it often requires operator intervention. Also the contour's shape depends on the number of markers. Recently, in order to avoid the over-segmentation problem, fuzzy relations were defined to sequence regions with similar grey value level under the constraint that only adjacent regions can be merged [16-17].

Another interesting approach is based on the use of active contours [18] which are topologically adaptable. Their inherent continuity and smoothness can in principle compensate for noise, gaps and spot boundary irregularities. The segmentation process of an image ( ) is based on the use of a piecewise parameterised curve C: [0, 1] $\rightarrow \mathrm{R}^2$. Then the energy associated with the contour is minimized:

$$\psi(c^+, c^-) = \mu \cdot length(C) + \lambda^+ \int_{inside(C)} | I(x, y) - c^+ | dxdy + \lambda^- \int_{outside(C)} | I(x, y) - c^- | dxdy \quad (1)$$

where c^+ and c^- represents the average intensities of $I(a, y)$ in the foreground and in the background respectively and μ, λ^+ and λ^- are regularizing parameters. The first term can be interpreted as the force which shrinks the contour while the second term expands it. The contour C evolves under the action of these two forces. The forces get balanced when the contour reaches the boundary of our interested object. The termsc^+ and c^- are iteratively updated during the evolution of the contour C. The process must start with contour initialization, which implies the rough identification of spots. Unfortunately the active contour is not completely insensitive to initialization [19]. Histogram adaptation and morphological reconstruction may be also necessary to avoid unwanted amplification of noise and streaks, as well as to facilitate the identification of faint spots [20]. Morphological operations have to be implemented using structuring elements, with shape and size in accordance with the shape of the spots.

Since the task of the present study is mainly exploratory and the nature of the spots on the divertor tiles is not yet precisely defined, the spot identification and characterization should not use any prior assumption regarding the size, shape and distribution of spots in order to preserve all the possible relevant information. Therefore it would be desirable to avoid methods which minimize the use of operators that may alter their shape (like e.g. median filtering, structuring elements with particular shapes, etc.). As the spot detection should be applied to the analysis of a large number of images, with variable brightness, contrast and noise level, a low parametric method, able to tackle these objectives must be used.

The main techniques discussed in the previous overview have been tested with typical videos produced by JET KL-9B camera and they have all shown significant limitations. The watershed tends to lead to over-segmentation in the presence of background non-uniformity. The active contour methods depend on the determination of several parameters. These parameters vary when the background varies significantly from an image to another, a typical problem in the case of the surveying of videos collected over long times in different experimental conditions. The use of specific structuring elements is prone to altering the shapes of the spots, causing difficulties in the interpretation of the results. A specific method for the spot detection in the frames of JET videos has therefore been developed and a description of its main elements is the subject of next section.

3. THE DEVELOPED SPOT DETECTION METHOD

In this work we introduce a simple semi-empirical method which does not use prior assumptions about the spots characteristics. The first stage consists of the determination of local intensity maxima. An efficient approach for this task is the maximum-minimum (MAX-MIN) filter, currently used in signal processing and pattern recognition. An efficient algorithm, requiring no more than 3 comparisons per element in the worst case, and which reduces the computer latency and memory usage was introduced in Ref. 21. Given an array $A = \{a_1,..., a_2\}$, the maximum and the minimum are found over all windows of size w, that is $\max/\min_{i\in[j,\,j+w]} a_i$ for all values. A monotonic wedge, made of two queues U, L, is maintained during the whole process. U and L satisfies:

$$\max_{i > U_{j-1}} a_i = a_{U_j}$$
$$\min_{i > L_{j-1}} a_i = a_{L_j} \qquad (2)$$

for $j = 1,2,...$where, by convention, $U_0 = L_0 = -\infty$.

The process starts with empty double ended queues which are updated by appending elements to 'back'. While traveling through the array A, if $i > w$ then $a_{front\ (U)}$ is the maximum of the range $[i - w, i)$ and $a_{back\ (L)}$ is the minimum of the range $[i - w, i)$. Traveling inside the window of size w and when inspecting the new element $a_{i,\ U}$, is popped from back while $a_i > a_{back\ (U)}$ and L is popped from back while $a_i > a_{back\ (L)}$. The monotonic wedge keeps the location of the current (global) maximum (U_1) and minimum (L_1) while it can be easily updated by removing data points from the left or append them from the right.

All pixels around the local maxima , with the intensity above a certain threshold , are classified as potentially belonging to the spot. This potential classification is validated only if:

- At a maximum distance d_{max} from the I^{local}, the gray level falls below the threshold T_1. This condition limits the size of the spots and d_{max} can be chosen in agreement with the experimental observations.
- The ratio between the grey level corresponding to the local maxima (GL_0) and the average grey-level (GL_{ave}) corresponding to the neighbouring pixels, potentially belonging to the spot, is above a certain threshold T_1: $\frac{GL_0}{GL_{ave}} > T_2$. This condition prevents the classification of flat regions as spots. It represents the only prior assumption about the shape of the spots – peak shape – but this assumption is derived directly from the experimental observations.

The spot identification depends on 3 adjustable parameters: T_1, T_2 and d_{max}. The last two parameters have a fixed value for all the images ($T_2 = 1.1$ and $d_{max} = 5$ pixels in our application). Unfortunately the parameter depends on the average gray-level in the image. This dependence has been determined empirically from visual inspection of the database. A set of 25 images with APGL covering the whole range observed experimentally $APGL \in (40 \div 140)$ has been chosen. Then the threshold T_1 has been manually adjusted for obtaining a 'good' spot detection. The quality of the spot identification has been judged by visual inspection. An example of the results obtained after the manual adjustment of T_1 is given in Fig.5.

The dependence of the threshold value T_1 with respect to the average grey-value has been obtained by a linear fit and it is presented in Fig.6 (red curve).

Overestimation of T_1 leads to spots with a too small area, or to missed spots, while the underestimation of this parameter leads to oversized spots, as illustrated in Fig.7. An initial T_1 underestimation is preferable. Taking into account the already used assumption that the spots area is below a certain limit A_{max}, the algorithm progressively increase T_1 the value, until all the spots areas are below A_{max}. In order to allow initial values of T_1 close, but below to the desired value, the

calibration curve describing the dependence of T_1 versus. the average gray-level is shifted to a parallel lower line (see Fig.6 – green curve). For all the experimental points, the corresponding T_1 values are higher than the value provided by the shifted calibration curve for the same APGL value. The initial T_1 value, corresponding to the shifted calibration curve, is gradually increased while all the spots areas are below A_{max} in steps of 5 units. The value of $A_{max} = 30$ has been determined by inspecting the available image database. The quality of this automatic procedure is illustrated in Fig.8. Spots identification by the automatic determination of T_1 is compared with the results obtained by the manual tuning of this parameter. The comparison covers the whole range of APGL values. Table 1 gives the characteristics of the images used in this comparison and the threshold values of T_1. The quality of spot identification decreases for an average gray-level above 156, for both manual and automatic T_1 determination. This imposes a criterion for the selection of the images provided by the KL-9B camera.

It must be noticed that sudden changes of the brightness in a sequence of images, corresponding to a specific pulse, may be due to the occurrence of plasma instabilities which produce light signals (such as e.g. ELMs). It is important to remark that this aditional illumination of the video scene can show an increased number of spots (part of them become invisible after the end of this transient phenomena). The ratio of the spots area with and without aditional illumination may differ by a factor of ~2.5. An example is given in Fig.9.

Unfortunately, as it is correlated with a certain magnitude of the plasma instability, this enhanced illuminations occur heratically and are very rare. Only seven cases have been identified for the total set of analyzed pulses. Moreover, the enhanced brightness occur more often in a limited region of the image. Even if they reveal more detailed information, these cases must be excluded from the analysis in order to have a uniform treatment of all images.

The spot identifcation techniques previously described must be preceeded by image registration, with respect to a reference frame, in order to compensate for camera movements, which quite frequently affect JET cameras. The registration is performed once for each image sequence corresponding to a JET pulse. We have used bright images able to reveal the sharp structures, adequate for retrieving Scale Invariant feature Transform (SIFT) detectors [22] – Fig.10. Seven significant changes in camera position (mainly vertical shifts) have been detected in the JET pulse history analyzed in this work which starts with the Pulse No: 80380 and ends with the pulse 83165 (see next section).

Since the spot patterns change significantly at relatively long time intervals, a procedure for identifying their evolution had to be devised. Illustrative examples are presented in Fig. 11. To this end, the spot distribution patterns have been determined for all the available images.

Then the correlation coefficient between the spot patterns corresponding to two successive images:

$$corr = \frac{N^2 \Sigma_i f_i^{k-1} - \Sigma_i f_i^k \Sigma_i f_i^{k-1}}{\left[N^2 \Sigma_i (f_i^k)^2 - (\Sigma_i f_i^k)^2\right]^{1/2} \left[N^2 \Sigma_i (f_i^{k-1})^2 - (\Sigma_i f_i^{k-1})^2\right]^{1/2}} \quad (2)$$

where N is the total number of pixels in the image and is the index of the current image, are calculated for all image pairs while travelling through each video. This coefficient has the value 1 for identical images. The evolution of the correlation coefficient displays several peaks which correspond to high correlation between spot patterns. This permits the determination of sequences of images for which the structure of spot patterns remain approximately unchanged. Spots with an area less than three pixels are removed in order to retain only the evolution of significant features. After sequence identification, all images in a sequence are summed and the resulting image is thresholded at 0.7 of its maximum grey-level. The thresholded image is considered to represent the characteristic pattern structure for a cluster.

4. ANALYSIS OF JET DATABASE OF VIDEOS

The pattern identification method has been applied to JET pulse history which starts with the Pulse No: 80380 and ends with the Pulse No: 83165. It was initially intended to travel through this history with a time step of 10 pulses. However for several periods of time KL-9B camera videos are not available or they consist of image sequences for which the region of interest corresponding to the divertor tiles is saturated and does not permit the spots visualization. Therefore a total number of 190 videos has been analyzed. The distribution of these pulses in time is presented in Fig.12.

After spot identification, the information which may be in principle correlated with the physical parameters of the discharges is retrieved. The evolution of the total spot area covering the divertor tiles has been calculated and it is represented in Fig. 13. The histogram of the spots area is presented in Fig.14.

The evolution of the correlation coefficient (Eq.2) has been evaluated for images corresponding to successive pulses along the history of experiments and it is illustrated in Fig.15 for the left divertor tile.

The peaks appearing in this evolution correspond to the formation of sequences of images with similar spot distributions. For each cluster, as explained previously, a representative pattern-image has been created by summing all the images in the sequence and thresholding the resulting image.

This procedure allows the identification of time intervals for which the distribution of spots remain approximately unchanged. This is illustrated in Figs.16-17 for both tiles. For the left tile, the multi-peak structure of the correlation coefficient, presented in Fig. 15 (between Pulse No's: 81290 and 81526), is explained by the slightly changes of the pattern structure. The occurrence of a giant spot is revealed for the right tile between Pulse No's: 82010 and 82128. The comparative clusterization for the two tiles is presented, together with the corresponding diagram of analysed pulses in Fig.18.

5. INTERPRETATION, CONCLUSIONS AND FUTURE WORK

A specific semi-empirical technique method for the spot detection in the frames of JET IR videos has been developed. It depends on only three parameters and only one of them has to be modified,

depending on the image brightness, according to a procedure which is described in the paper. The method does not use any prior assumption regarding the spots parameters and distribution, allowing the preservation of the irregular shapes. Spot distribution evolution during the JET pulse history is followed by the identification of the correlations of these distributions with the physical parameters of the experiments.

With regard to the interpretation, the situation is a bit more involved. The nature and origin of the detected spots are not clear. They are believed to be due to the interaction between the tiles and dust mobilized during the discharges. This interpretation seems reasonable, since a limited number of flying dust particles have indeed been detected. On the other hand, the detected spots are rigorously stationary during the discharges and therefore their nature will have to be confirmed by appropriate post mortem analysis.

The correlation between the distribution of the spots and macroscopic events has been investigated. The abrupt of the correlation between subsequent discharges has been found to correlate with shot intervals characterized by a series of intentional disruptions and related studies (such as massive gas injection). This is illustrated in Fig. 19, which relates the main variations in the correlation coefficients with the main features of the corresponding experimental programme.

A word of caution about the interpretation is also in place. An almost identical camera is located on a different toroidal location in JET. It is called KL-9A and it is meant to study the toroidal asymmetries of the IR radiation from the divertor. Unfortunately, due to different settings, in many cases the images provided by the KL-9A camera are characterised by a very high saturation, which usually makes impossible the spot visualisation. Therefore a complete statistical comparison is not possible. On the other hand, for all the limited cases in which an acceptable video is available, the differences between the KL-9B and KL-9A frames are striking. The number and distribution of the spots are completely different, as exemplified in Fig. 20. Therefore the generalization of the results obtained by only one toroidal view is not granted by the evidence, even if limited, of a different toroidal view. It is also worth noting that other evidence of toroidal asymmetries in the power deposition on JET, such as toroidal localized melting of poloidal limiters, has been recently collected [23]. A more systematic comparison between the two cameras will have to be undertaken in the future to obtain clear indications about the total distribution of these spots in JET divertor.

ACKNOWLEDGMENT

This work was supported by the European Communities under the contract of Association between EURATOM and MEdC, ENEA and IPP and was carried out within the framework of the European Fusion Development Agreement. The views and opinions expressed herein do not necessarily reflect those of the European Commission.

REFERENCES

[1]. G.F. Matthews, M. Beurskens, S. Brezinsek, M. Groth, E. Joffrin, A. Loving, M. Kear, M.-

L. Mayoral, R. Neu, P. Prior, V. Riccardo, F. Rimini, M. Rubel, G. Sips, E. Villedieu, P. de Vries, M.L. Watkins, JET ITER-like wall—overview and experimental programme, Physica Scripta 2011, **T145**, 014001 doi:10.1088/0031-8949/2011/T145/014001.

[2]. I.Balboa, G. Arnoux, T. Eich, B. Sieglin, S. Devaux, W. Zeidner, C. Morlock, U. Kruezi, G. Sergienko, D. Kinna, P.D. Thomas, M. Rack, Upgrade of the infrared camera diagnostics for the JET ITER-like wall divertor, Review of Scientific Instruments, **83**-10(2012)10D530.

[3]. M. Berth, F.M. Moser, M. Kolbe, J. Bernhardt, The state of the art in the analysis of two-dimensional gel electrophoresis images, Applied Microbiology and Biotechnology (2007) **76**:1223–1243

[4]. C.-L. Shih, H.-W. Chiu, Automatic spot detection of cDNA microarray images using mathematical morphology methods, IEEE EMBS Asian-Pacific Conference on Biomedical Engineering, 2003, pp. 70-71.

[5]. A.B. Kadam, R.R. Manza, K.V. Kale, A Novel Approach For Microarray Spot Segmentation and Detection Using Four Shaped Mathematical Morphology, Advances in Computational Research, ISSN: 0975-3273 & E-ISSN: 0975-9085, Volume **4**, Issue 2, 2012, pp.-130-133.

[6]. I.Smal, M. Loog,W.J. Niessen, E.H.W. Meijering, Quantitative comparison of spot detection methods in live-cell fluorescence microscopy imaging, IEEE International Symposium on Biomedical Imaging: From Nano to Macro, 2009. ISBI '09, pp. 1178-1181.

[7]. S.H. Rezatofighi, R. Hartley, W.E. Hughes, A new approach for spot detection in total internal reflection fluorescence microscopy, 9th IEEE International Symposium on Biomedical Imaging (ISBI), 2012 pp. 860– 863.

[8]. G. Cuartero, V. Meas-Yedid, V. Galy, U. Nehrbass, J.-C. Olivo-Marin, Three dimensional spot detection by multiscale analysis, International Conference on Image Processing, 2001, Vol. **1**. Pp. 317-320.

[9]. M. Tello, C. López-Martínez, J. Mallorquí, R. Bonastre, Automatic Detection of Spots and Extraction of Frontiers in SAR Images by Means of the Wavelet Transform: Application to Ship and CoastlineDetection, IEEE International Conference on Geoscience and Remote Sensing Symposium, 2006. IGARSS 2006. pp. 383 – 386.

[10]. M. Côté, P. Hurat, Standard cell printability grading and hot spotdetection, Sixth International Symposium on Quality of Electronic Design, 2005. ISQED 2005, pp. 264 – 269.

[11]. R.F. Salem, A. Arafa, S. Hany, A. ElMously, H. Eissa, M.A. Dessouky, D.G. Nairn, M.H. Anis, A parametric DFM solution for analog circuits: Electrical driven hot spot detection, analysis and correction flow, IEEE International SOC Conference (SOCC), 2011, pp. 231 – 236.

[12]. P. Saripalli, G.V.R. Kiran, R.R. Shankar, H. Narware, N. Bindal, Load Prediction and Hot Spot Detection Models for Autonomic Cloud Computing, Fourth IEEE International Conference on Utility and Cloud Computing (UCC), 2011, pp. 397 – 402.

[13]. Y. Kim, J. Kim, Y. Won and Y. In, "Segmentation of Protein Spots in 2-D Gel Electrophoresis Images with Watershed Using Hierarchical Threshold," LNCS, vol. **2869**, pp. 389-396, 2003.

[14]. S. Beucher, C. Lantuéjoul, Use of watersheds in contour detection, In International workshop on image processing, real-time edge and motion detection. http://cmm.ensmp.fr/~beucher/publi/watershed.pdf.

[15]. F. Meyer, S. Beucher, Morphological segmentation, The watershed transformation applied to image segmentation, J. Vision Comm. Image Roy. 1(1990)21–46.

[16]. L. Patino, Fuzzy relations applied to minimize over segmentation in watershed algorithms, Pattern Recognition Letters **26** (2005) 819–828.

[17]. S. Rashwan, T. Faheem, A. Sarhan, B., A.B. Youssef, A Fuzzy-Watershed Based Algorithm for Protein Spot Detection in 2DGE images, IJCSNS International Journal of Computer Science and Network S 254 Security, VOL.10 No.5, May 2010, pp. 254-257.

[18]. T.F. Chan and L.A. Vese, Active Contour Without Edges, IEEE Trans. Im. Proc., vol. **10**, no. 2, pp. 226-277, 2001.

[19]. S.H. Lee, J.K. Seo, Level set-based bimodal segmentation with stationary global minimum, IEEE Trans. Image Process. 15-9(2006)2843–2852.

[20]. M.A. Savelonas, E.A. Mylona, D. Maroulis, Unsupervised 2D gel electrophoresis image segmentation based on active contours, Pattern Recognition 45-2(2012)720-731.

[21]. D. Lemire, Streaming Maximum-Minimum Filter Using no more than Three Comparisons per Element, Nordic Journal of Computing, Volume **13**-4(2006)328-339.

[22]. D.G. Lowe, Distinctive Image Features from Scale-Invariant Keypoints, International Journal of Computer Vision, **60**-2(2004)91-110.

[23]. A. Widdowson, E. Alves, C.F. Ayres, A. Baron-Wiechec, S. Brezinsek, J.P. Coad, K. Heinola, J. Likonen, G.F. Matthews, M. Rubel, Material Migration Patterns and Overview of First SurfaceAnalysis of the JET ITER-like Wall, to be presented at 14th International Conference on Plasma-Facing Materials and Components for Fusion Applications, 13-17 May 2013, Juelich, Germany.

JET Pulse No: *Frame* *Tile*	*82173* *1197* *Left*	*82173* *1197* *Right*	*81423* *503* *Left*	*81423* *503* *Right*	*81423* *1043* *Right*	*80450* *2437* *Right*
Average gray-level	*44*	*66*	*83*	*114*	*137*	*156*
T_1 – manual tuning	*100*	*125*	*145*	*180*	*207*	*230*
T_1 – automatic procedure	*107*	*127*	*142*	*178*	*209*	*234*

Table 1: Average gray-levels and T_1 values for the images in Fig.4.

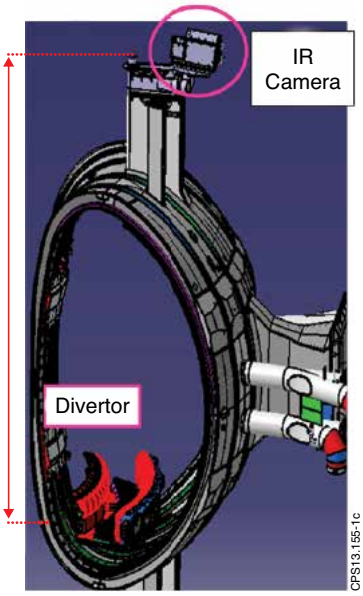

Figure 1: The IR camera located on top of JET to see the divertor.

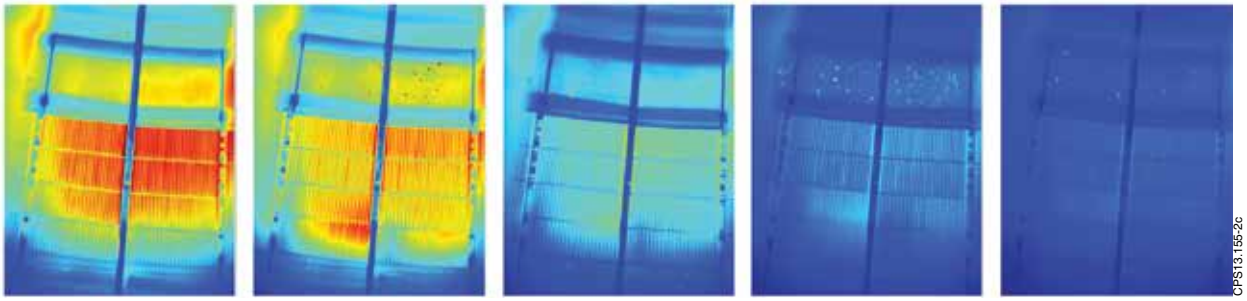

Figure 2: Typical images recorded by the JET KL-9B camera.

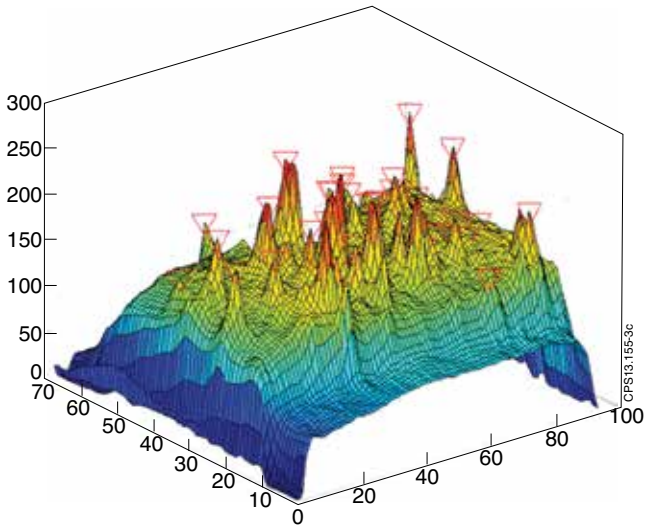

Figure 3: Intensity of the spots on the variable intensity background.

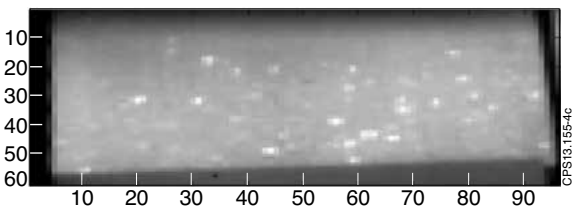

Figure 4: Typical spot distribution recorded on a divertor tile.

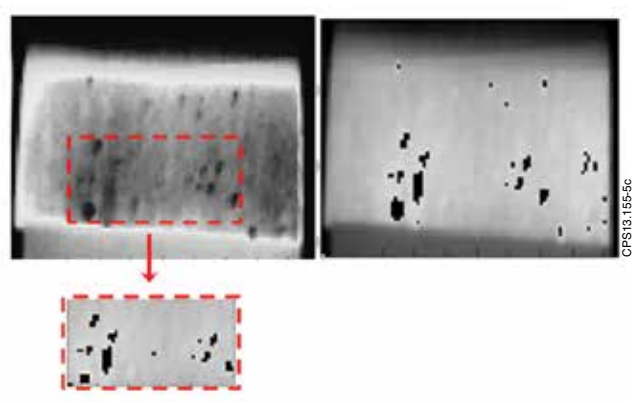

Figure 5: Illustration of the spot identification obtained using the manual adjustment of the parameter T_1.

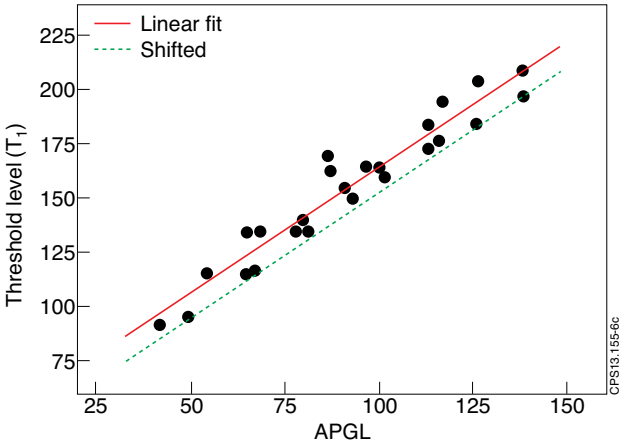

Figure 6: The dependence of the threshold parameter T_1 on the image pixel average gray-level APGL (red curve). This calibration curve is shifted to a parallel lower line (green curve) in order to get initial values of T_1 in the iterative process of adjusting this threshold level.

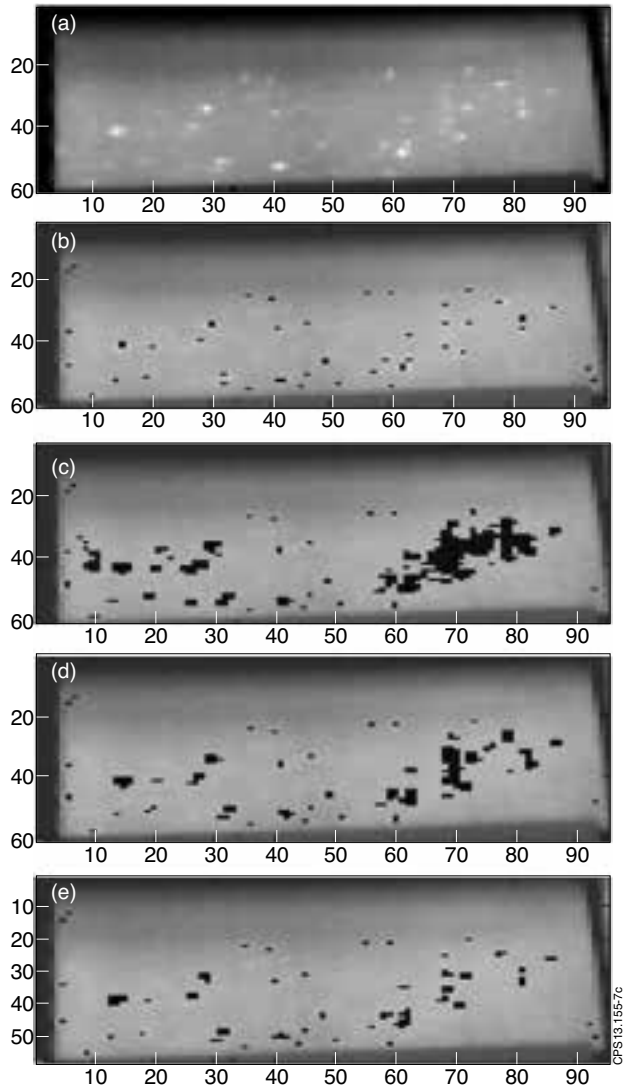

Figure 7: llustration of the effect of the variation on the spot identification: the original image – frame no. 503/ right tile recorded during JET pulse 81423 (A), spot identification using an overestimated value of (=210) (B), spot identification using an underestimated value of (C – =180, D – =190) and spot identification using a proper value of (=197). The effect of the progressive increase can be observed following the image sequence C-D-E.

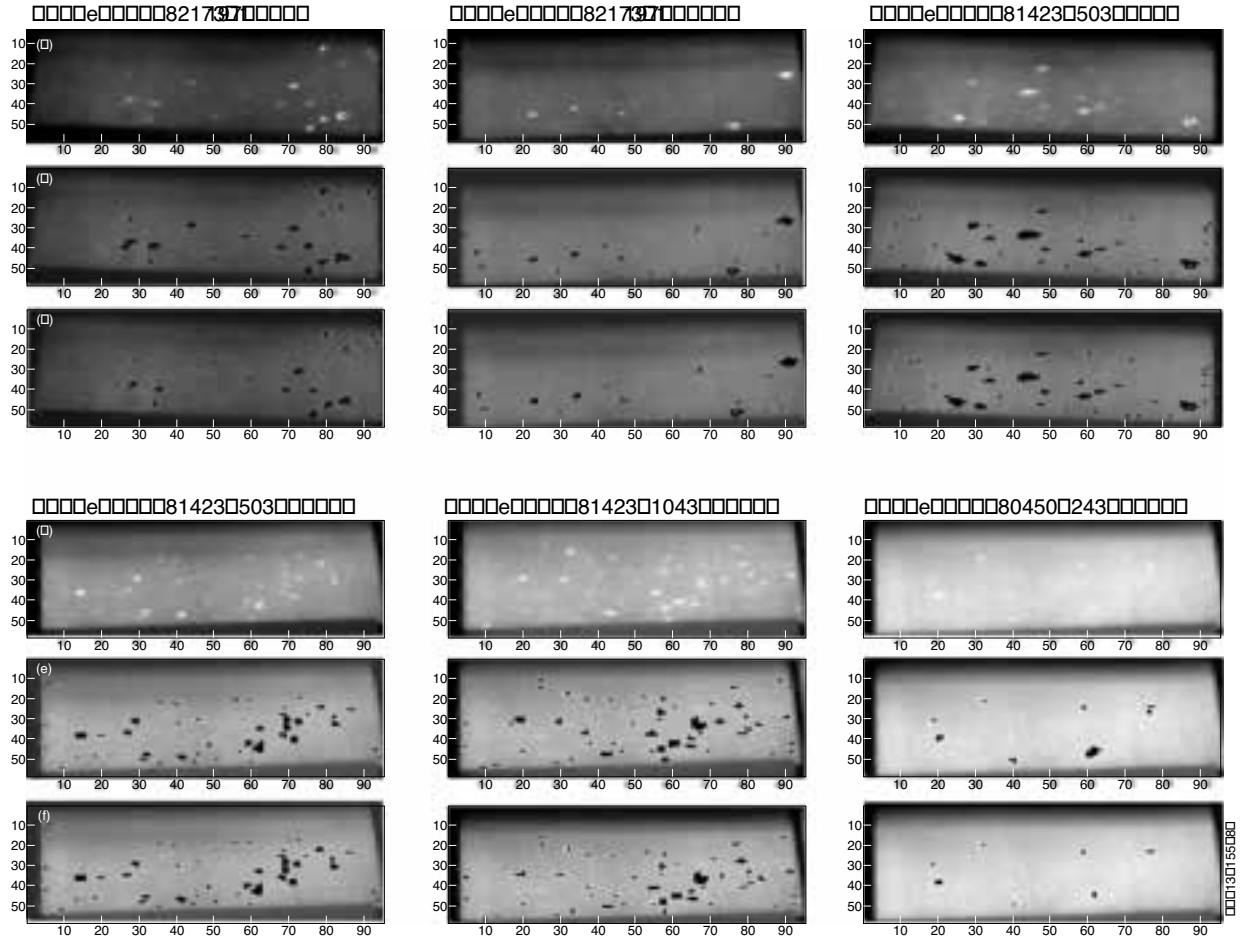

Figure 8: Illustration of the quality of the automatic procedure for T_1 determination: original images (A), spot identified by T_1 manual tuning (B) and by using the automatic procedure for T_1 determination (C). JET pulse / frame no / and tile are indicated for each image.

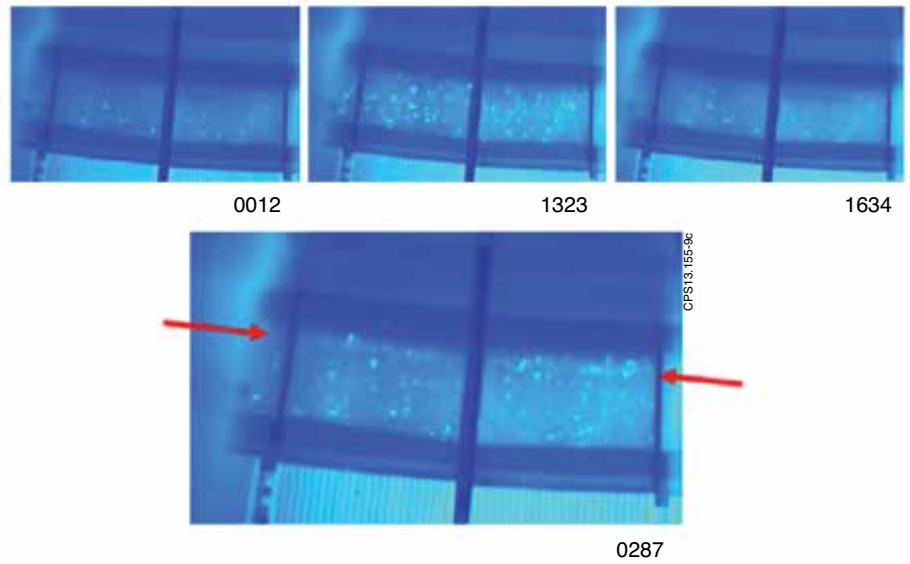

Figure 9: Illustration of the effect induced by a temporary brightness enhancement due to an ELM. A sequence of three images, corresponding to the JET Pulse No: 81148, where the effect is clearly visible, for the whole image, for the frame no. 1323, is shown on the top of the figure. The enhanced illumination may appear on a limited area of the image as indicated by the red arrows on the bottom of this figure.

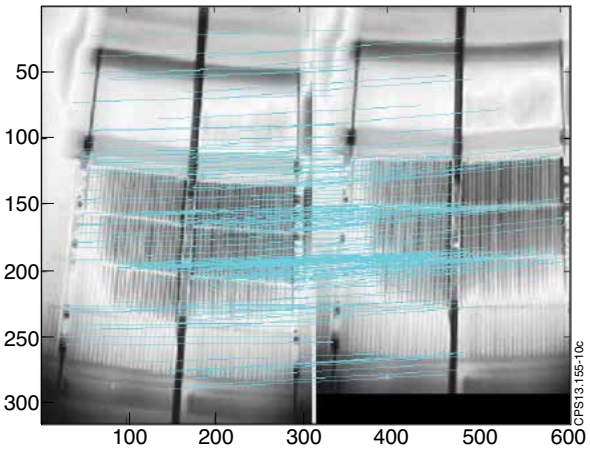

Figure 10: mage registration using SIFT detectors. Bright images permit the identification of a large number of points of interest allowing a precisely determination of amount of image shift and rotation.

Figure 11: Examples of the spot distribution pattern

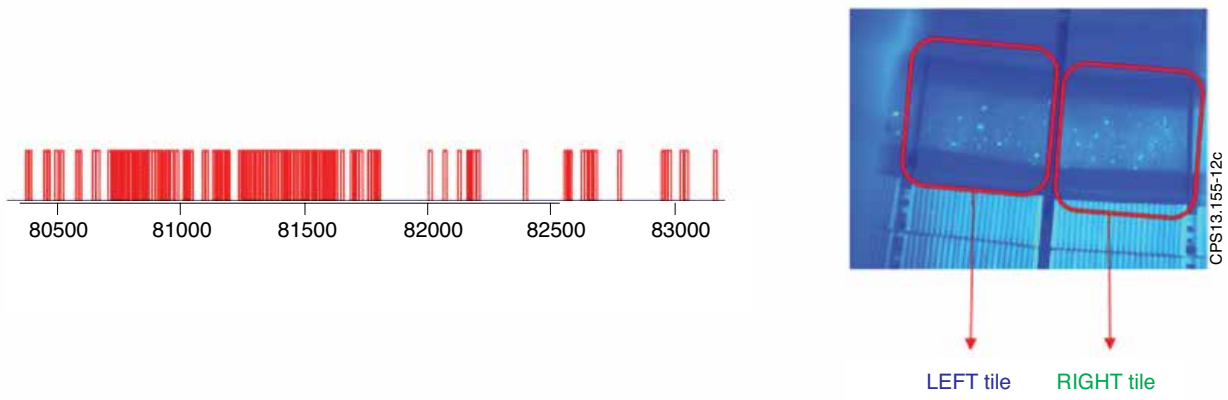

Figure 12: The distribution of the analyzed JET pulses as a function of shot number (left). The analysis has been performed separately for the two divertor tiles

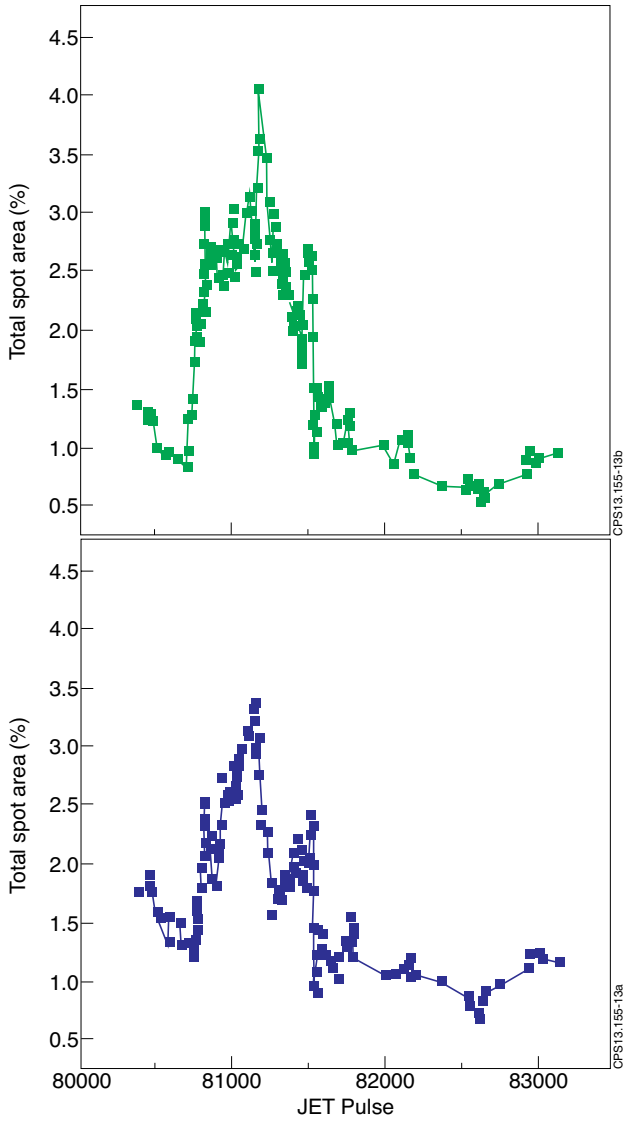

Figure 13: The evolution of the total spot area for the left divertor tile (top) and for the right one respectively (bottom). The diagram showing the distribution in time of the analysed pulses in shown in the middle of this figure.

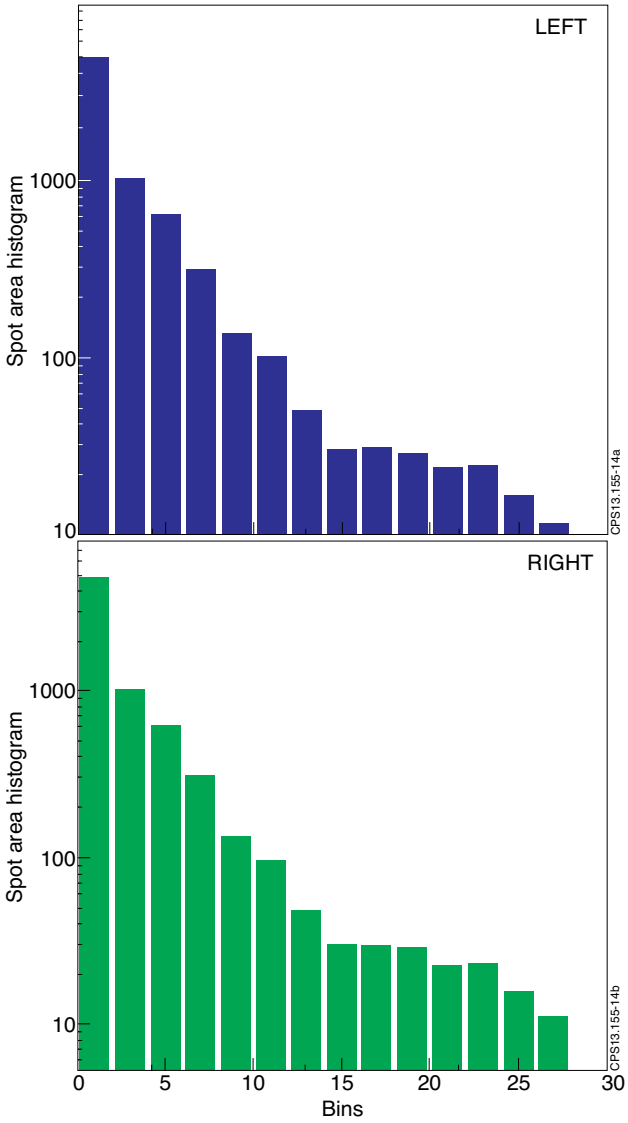

Figure 14: The histogram of the spot area for the left divertor tile (top) and for the right one respectively (bottom).

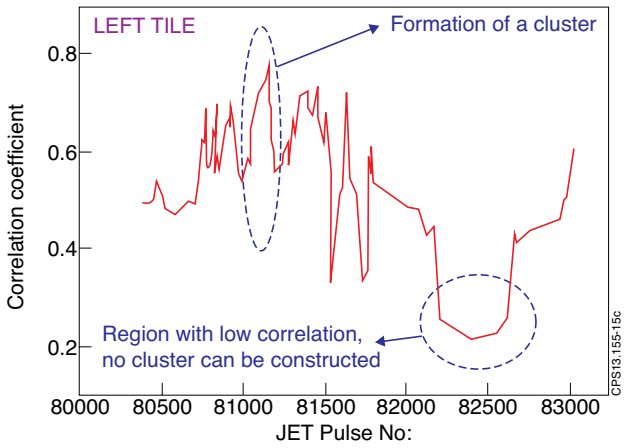

Figure 15: The evolution of the correlation coefficient between spot patterns corresponding to successive JET pulses. The peaks appearing in this evolution corresponds to the formation of sequences of images with similar spots distribution. A low value of the correlation coefficient corresponds to images with significantly different spots distribution.

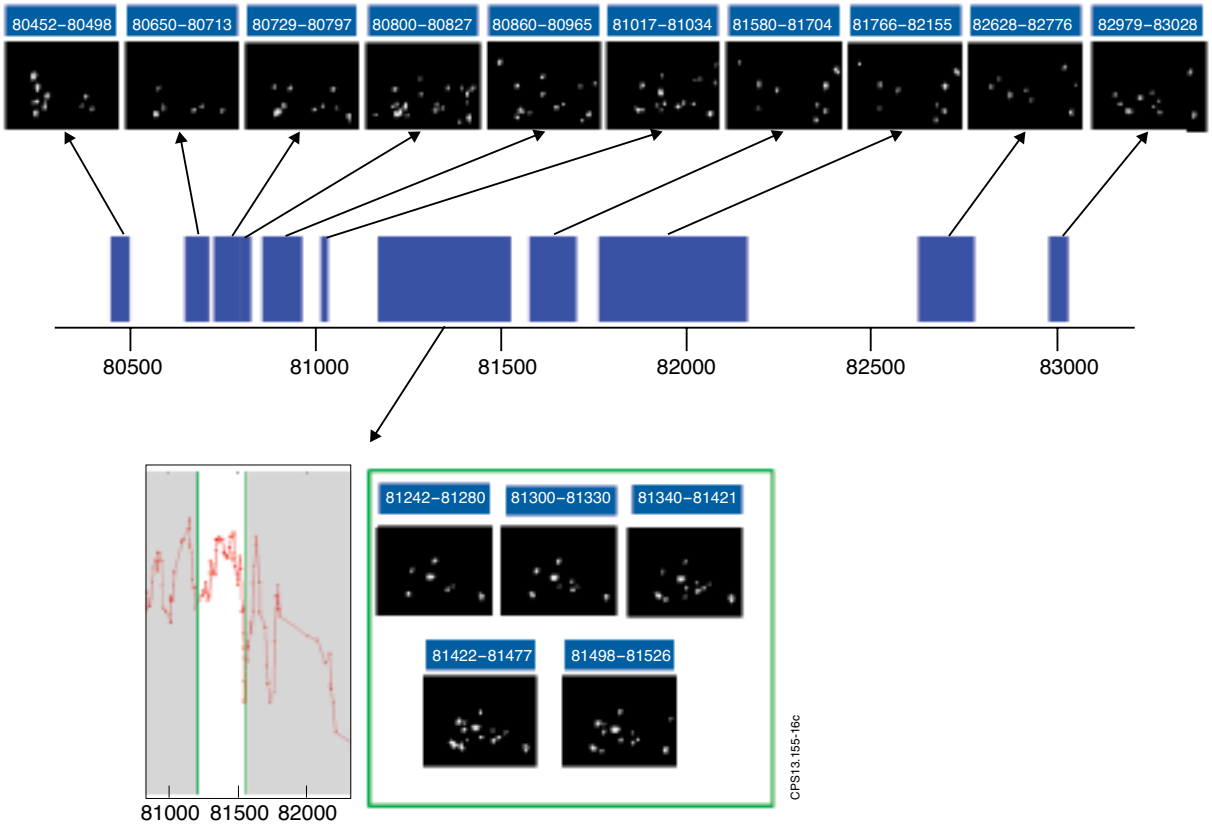

Figure 16: The spots pattern evolution for the left divertor tile (top). During the time interval starting with Pulse No: 81290 and ending with the Pulse No: 81526 the pattern structure changes slightly as revealed by the multi-peak structure of the correlation coefficient corresponding to this time interval (bottom).

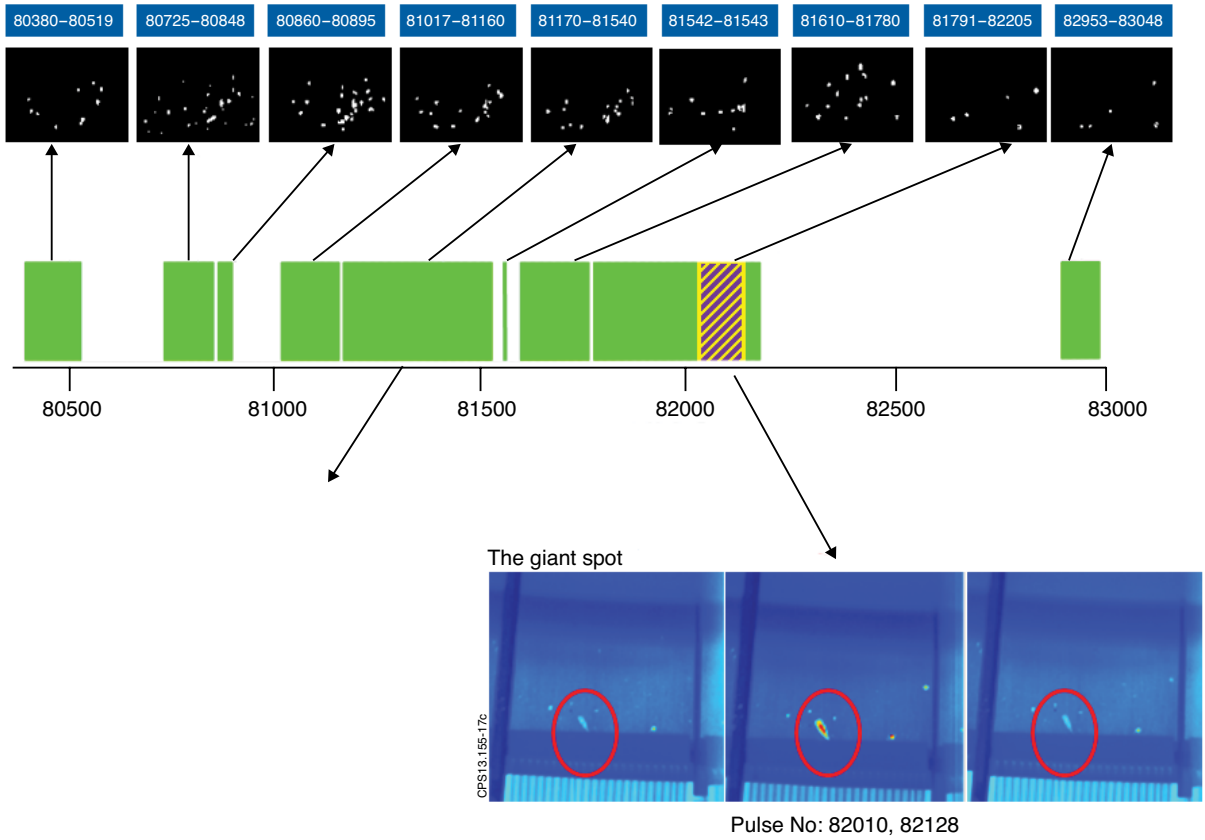

Figure 17: The spots pattern evolution for the right divertor tile (top). A giant spot appeared between JET Pulse No's: 82010 and 82128.

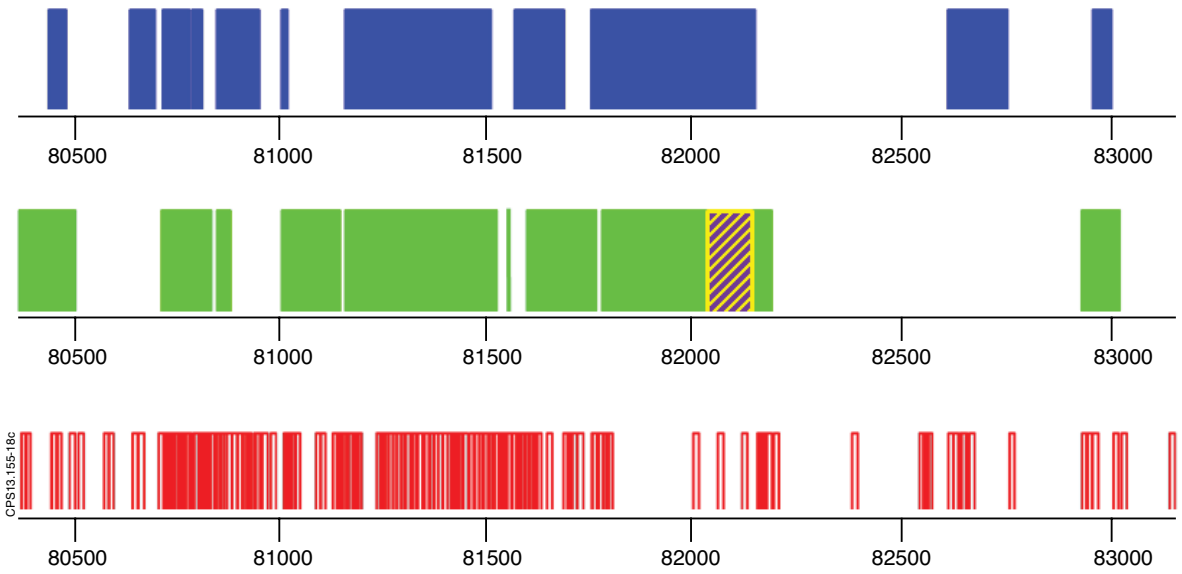

Figure 18 : Comparative clusterization for the two divertor tiles - left tile (top), right tile (middle) – together with the diagram showing the distribution of the analysed pulses in time.

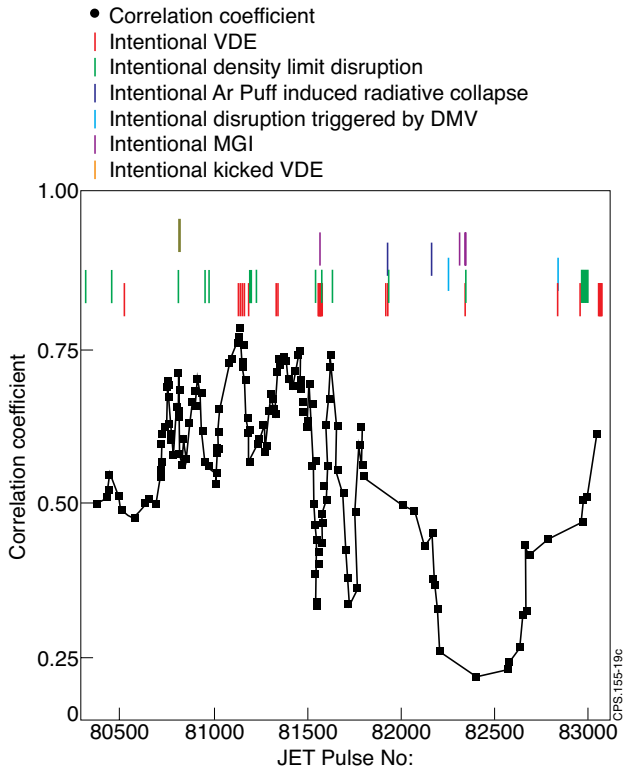

Figure 19: The relation between the abrupt reductions in the correlation coefficient and the experiments, mainly related to intentional disruptions. VDR: Vertical Displacement Events DMV: Diagnostic Mass Valve MGI: Massive Gas Injection

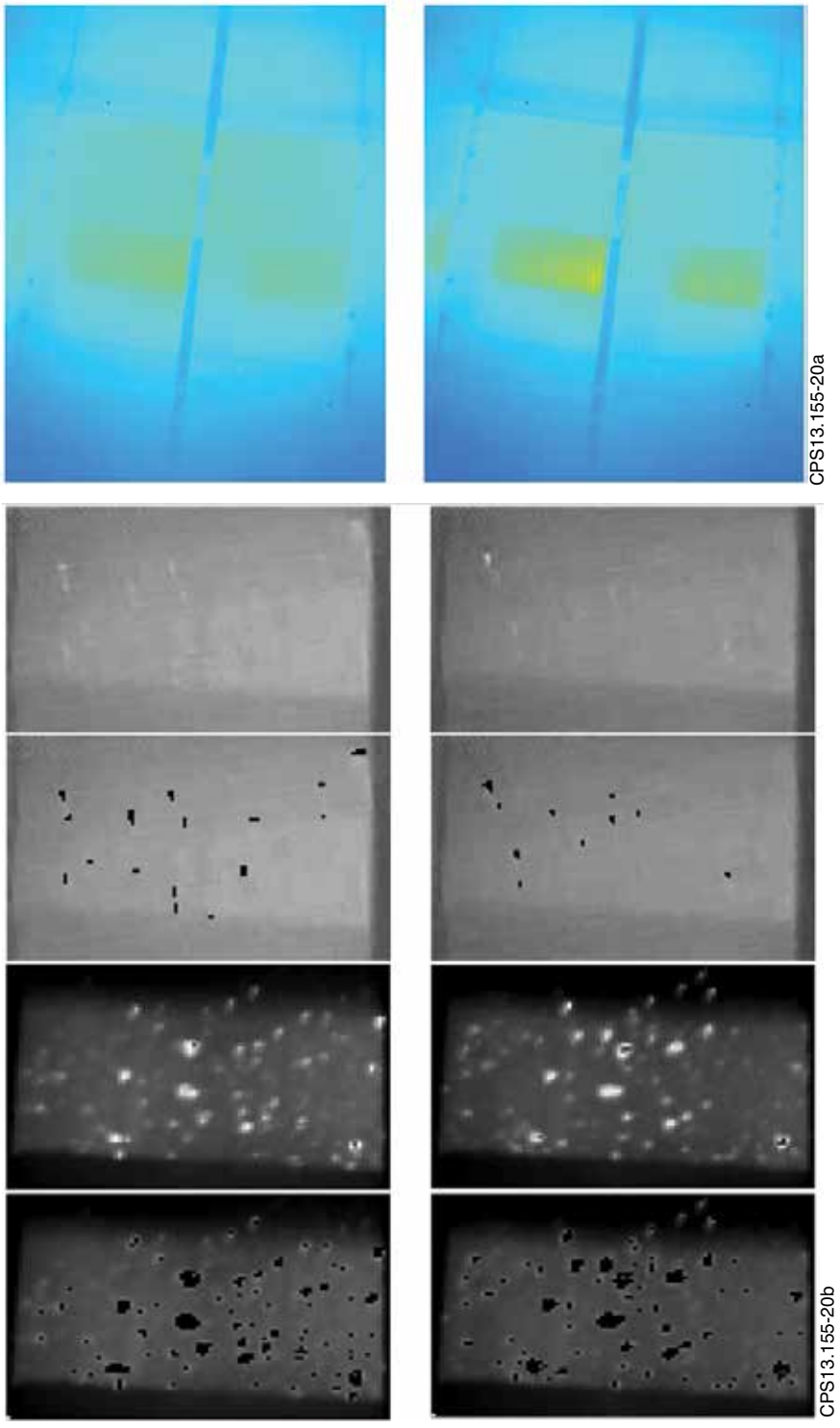

Figure 20: Comparison between spots pattern revealed by KL-9A and KL-9B cameras. The original KL-9A images corresponding to JET Pulse No's: 81145 and 81193 are presented in the first row. The left tile images, after histogram manipulation, are presented in the second row. The corresponding spots identification is presented in the third row. The forth row shows the left images retrieved by the KL-9B camera for the same JET pulses and the fifth row presents the corresponding spots identification. The left column presents corresponding related to the JET Pulse No: 81145 while the right one shows images corresponding to the JET Pulse No: 81193, respectively.